

A STUDY ON THE CHANGES IN MICROSTRUCTURE AND MECHANICAL PROPERTIES OF MULTI-PASS WELDING BETWEEN 316 STAINLESS STEEL AND LOW-CARBON STEEL

A.T. Hoang¹, V.V. Le¹, A.X. Nguyen² and D.N. Nguyen²

¹Faculty of Mechanical Engineering,
Ho Chi Minh city University of Transport, Ho Chi Minh, Vietnam.

²School of Mechanical Engineering,
Vietnam Maritime University, Haiphong, Vietnam.

Corresponding Author's Email: tuan.hoang@ut.edu.vn

Article History: Received 15 May 2018; Revised 8 August 2018; Accepted 24 September 2018

ABSTRACT: In this study, the changes in the microstructures and mechanical properties in the fusion zone and heat-affected zone (HAZ) of the welds between 316 stainless steel and low-carbon steel were investigated. The formation of the morphology of δ – Ferrite including the columnar dendritic and the equiaxed dendritic in either the single-pass welding or multi-pass welding was analyzed through SEM. The recrystallization phenomenon in two regions such as HAZ-1 with grain-refining and HAZ-2 with partial grain-refining was considered as the main cause leading to differences in the microstructure and mechanical properties of the above-mentioned welds. As a result, the hardness, tensile strength and elastic strength of multi-pass welding were higher than those of single-pass welding. The lower elongation of multi-pass welding compared to single-pass welding was also observed.

KEYWORDS: *Dissimilar Metal Weld; HAZ; Multi-Pass Welding; 316 Stainless Steel; Low-Carbon Steel*

1.0 INTRODUCTION

Arc welding is the process of heating a metal at the welding position to a melting state, after that the solidification process occurs to form a welding bond. The physical and chemical processes occurring in the weld are similar to the metallurgical process, however, because of the small area of the puddle, the solidification time is very short [1-3]. The temperature of the welding is very high (up to 3000°C for arc welding), thus, the metal at the welding is locally heated, and heat generated from the welding is transferred to the surrounding environment [4-6].

The temperature and cooling rates at each location in the weld metal zone and the heat-affected zone are different, leading to differences in microstructure and mechanical properties. Metal welds are illustrated in Figure 1, and divided into the following areas:

- i. Melting zone: The metal zone is heated to a complete liquid state with a similar microstructure to the casting after being solidified.
- ii. Thermal zone: It is the zone from the border of the melting to the positions with the temperature of 500°C.
- iii. Base metal: The areas with the temperature are less than 500°C.

These areas have the structures which are the same as the structures of the base metals but the residual stress still exists due to the influence of temperatures.

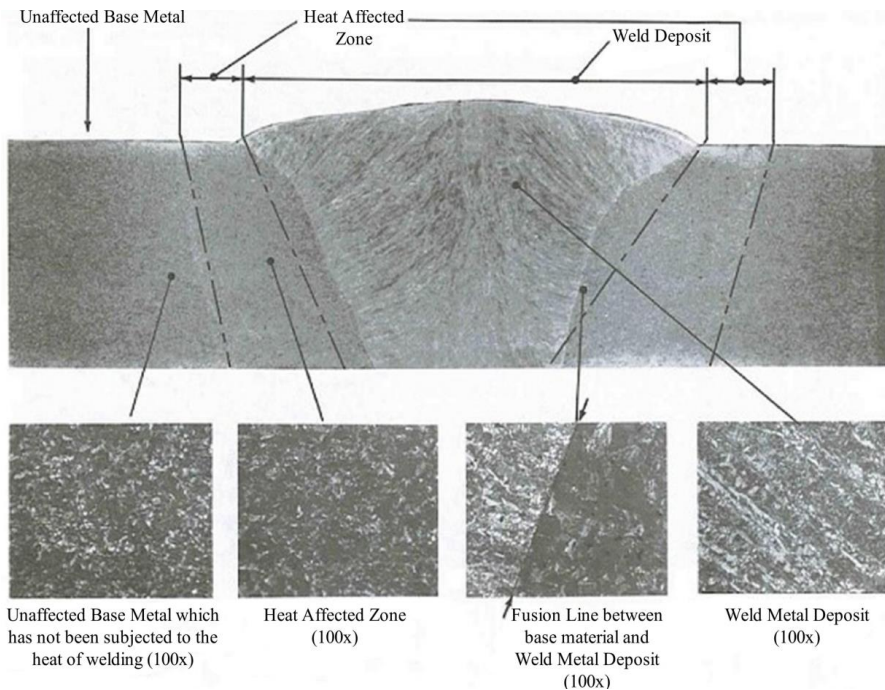


Figure 1: Microstructure of welding [7]

In fact, the joining of engineering components and the fabrication of mechanical parts are usually based on dissimilar metal welds (DMW) between austenite-based stainless steel and carbon steel. Nonetheless, it is difficult to control microstructures of metals in the weld as well as their properties. Particularly, the control of heat – affected zone (HAZ) is considered as a challenge for weld engineers. According

to literature, differences between the weld metals and base metals related to physiomechanical and metallurgical properties exist [8-12]. For example, the coefficient of thermal expansion of the weld metals is different from base metals, leading to locally-high stresses which promote the service failures because of the thermal cycles from low-temperature zones to high-temperature zones. Besides, differences in composition and microstructure may be the main cause resulting in the local variations of the corrosion resistance in either the weld metal or the transition region [13]. Normally, DMW components are conducted to weld the plates using multi-pass welding methods, aiming at ensuring the strength and the homogeneity of the microstructure between weld metals and base metals [14]. Generally, the single-pass weld characteristics are not so complex as those of multi-pass weld due to the effects of the thermal cycles of subsequent passes which impact strongly the mechanical properties (such as hardness, tensile strength, elastic strength, and elongation), the microstructure, and the residual stresses after heat treating or cooling to ambient temperature [15-16]. Thus, the use of the results from studies related to the thermal or heat treatment process, and distributions of the residual stress at the welding zones may be considered as an effective method to understand clearly the transformation of the phases, and physicochemical properties of the metals at/in the various zones of welds [17].

Evidently, there is a close relationship between the changes in microstructures and mechanical properties of the weld metals in the welding zones. The microstructures with the large residual stress may affect the mechanical properties of weld metal negatively especially in the fusion zone and HAZ. Therefore, the aim of this work was to study the changes in microstructures in the above-mentioned fusion zone and HAZ and the influences of those changes on the hardness, tensile strength, elastic strength, and elongation values of the single – pass and the multi-pass welds between 316 stainless steel and low-carbon steel.

2.0 MATERIAL AND EXPERIMENTAL SETUP

2.1 Material

In this experimental method, the as-used base metals were 316 stainless steel with 4mm of thickness and low-carbon steel with 20mm of thickness. The chemical composition of the 316 stainless steel and low-carbon steel along with the chemical composition of filler are illustrated in Table 1.

Table 1: The chemical composition

Alloys	C, %	Mn, %	Si, %	S, %	P, %	Cr, %	Ni, %	Mo, %	V, %
316 stainless steel	0.08	2.00	1.00	<0.03	0.045	18.5	10.2	1.95	0.02
Low-carbon steel	0.1	0.62	0.02	0.04	0.05	0.02	0.08	0.005	0.01
Filler	0.08	0.7	0.8	<0.005	<0.003	19.7	11.8	0.1	0.09

2.2 Experimental Setup

The preparation of welding shown in Figure 2 was based on the method of GTAW (Gas Tungsten Arc Welding) which was used for the root pass, the method of SMAW (shielded metal arc) was used for the following multi-pass welding, and the single-pass welding. The welding parameters of multi-pass welding and the single-pass welding are listed in Table 2.

Table 2: The welding parameters of the multi-pass welding

WELDING	Pass No.	Current (A)	Voltage (V)	Travel speed (mm/min)	Preheat/Inter-pass temperature (oC)	Shielding gas flow rate (l/min)
MULTI-PASS WELDING	1	93	50	16.8	61	12
	2	120	54	71	64	12
	3.1	99	22	45	57	-
	4.1	99	24	42	73	-
	4.2	111	24	56	54	-
	5.1	113	25	57	57	-
	5.2	115	25	48	64	-
	6.1	116	24	57	80	-
	6.2	113	24	62	89	-
	6.3	114	25	41	61	-
	7.1	116	24	55	73	-
	7.2	114	25	58	87	-
	7.3	110	24	55	89	-
	7.4	113	25	43	98	-
	7.5	110	25	43	106	-
SINGLE-PASS WELDING	1	100	25	12.0	25	-

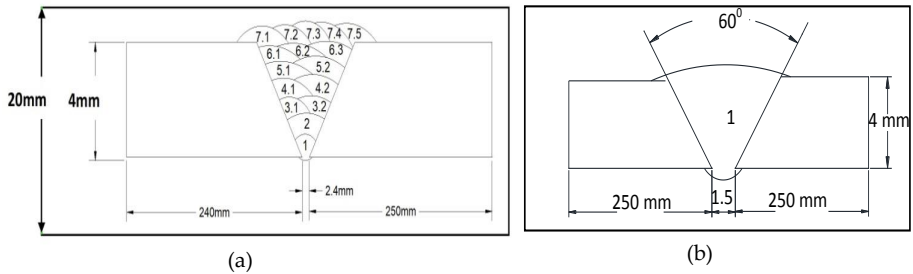


Figure 2: Welding preparation: (a) Multi-pass welding and (b) Single-pass welding

After welding under the as-used conditions, microstructures of weld metal zones and their characteristics were evaluated and determined using modern devices which include a WEW1000B machine for the test of transverse tensile, OMLEICA MDS4000M and FE-SEM (JSM7600F) for the test of microstructures and ARK600 machine for hardness value test. However, before testing, samples were mechanically polished and enchanted by a solution containing 3% of HNO_3 for low-carbon steel. The above-mentioned mechanical polishing way used for 316 stainless steel and weld metal was a solution containing 5g of FeCl_3 , 15cm^3 of HCl , which was diluted by 100cm^3 of H_2O , hydrochloric acid, and alcohol.

3.0 RESULTS AND DISCUSSION

3.1 Multi-Pass Welding Macrostructure

The findings yielded that the as-used base metals were austenite-based 316 stainless steel and low-carbon steel. Thus, small regions of Pearlite and Ferrite can be observed as shown in Figure 3a, and be considered as the typical microstructure of low-carbon steel whereas microstructures of 316 stainless steel showed the austenite-based phases as illustrated in Figure 3b.

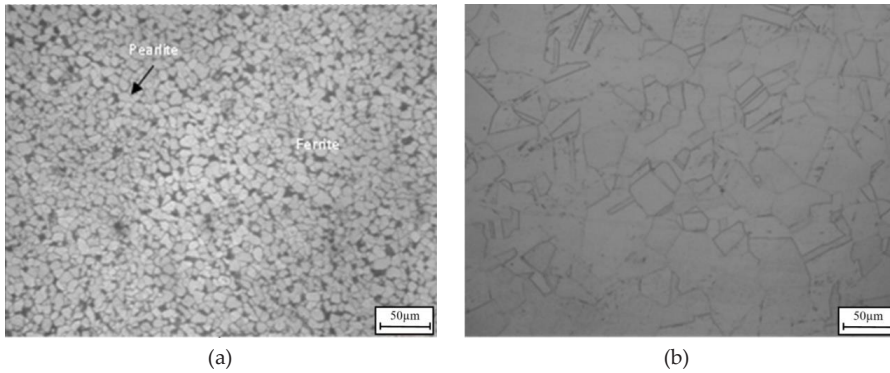


Figure 3: Microstructure of the base metals: (a) Low-carbon steel and (b) Austenite-based 316 stainless steel

After the DMW process was conducted, the microstructure of the welding zone showed a significant change in three different regions such as the HAZ, weld zone, and base-metal zone. The welding macrostructure based on multi-pass layers can be clearly seen in Figure 4. After the solidification process, δ -Ferrite-based phases were formed in the zones of the weld metal, and its morphology presented the fine cellular to continue the columnar dendritic transition. In the multi-pass welding, the HAZ recrystallization of low-carbon steel was classified, including HAZ-1, HAZ-2. However, no changes in the phase morphology in HAZ for austenite-based 316 stainless steel was seen.

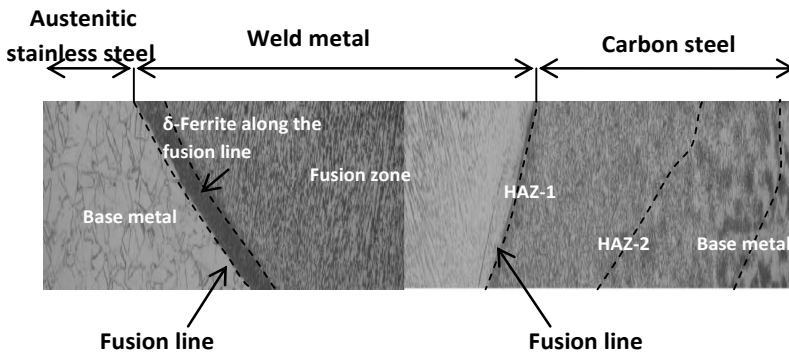


Figure 4: Macrostructure of the multi-pass welding

3.2 The Morphologies of Delta-Ferrite in the Fusion Zone

The difference of δ -Ferrite morphology was clearly seen in the fusion zone. While Figure 5a illustrates the single-pass welding, Figure 6 illustrates δ -Ferrite morphology for multi-pass welding. In the single-pass welding, the transformation of the δ -Ferrite phases from

fine cellular into the equiaxed dendritic and columnar dendritic was observed in the middle of weld metal and along the fusion line.

At the melting border of stainless steels (Figure 5b), the liquid metal began to crystallize from stainless steel. Because the structure of the liquid metal was the same as the structure of the base metal, the solid phase at the boundary was melted when parasitic nucleus were favorable for the crystallization. Liquid crystals are crystallized in the FA model, hence, the ferrite is released from the liquid phase.

The morphology of δ -Ferrite formed the thin strands growing up in a direction perpendicular to the melting border. However, due to the high cooling rate, the Widmanstätten austenite phases occurred along the melting front side of the stainless steel. Next, the morphology of the ferrite which was fish-shaped, was developed in a direction perpendicular to the melting border. In contrast, the morphology of δ -Ferrite formed on the melting carbon steel boundary was distinct (Figure 5c). Owing to the molten metal composition at the border carbon steel, the crystalline structure was Austenite (long white phase running along the melting border). The δ -Ferrite phase was released in the form of Anthracene on the Austenite base. Into the interior, due to the competitive development between δ - Ferrite and Austenite, δ -Ferrite had a branch shape in the direction of perpendicular direction of heat transfer. The morphology of δ - Ferrite on the Austenitic base in the center of the weld metal depended on the changes in temperatures. In the area close to the melted boundary, the superheat extended to form δ - the longitudinal spherical Ferrite that tended to direct in the center of the weld, and was perpendicular to the molten boundary (Figure 6a). In the center of the weld, the coolant decreased, and the temperature was uniform in all directions. The δ - Ferrite was a result of the spherical shape formation (Figure 6b).

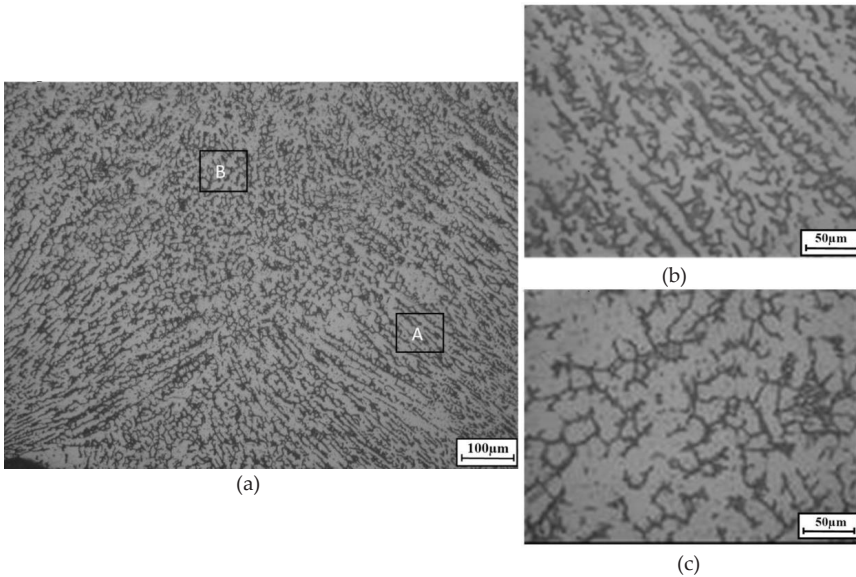


Figure 5: Microstructure in the fusion zone of single-pass welding: (a) Microstructure in the fusion zone, (b) Position A with the columnar dendritic δ -Ferrite and (c) Position B with the equiaxed dendritic δ -Ferrite

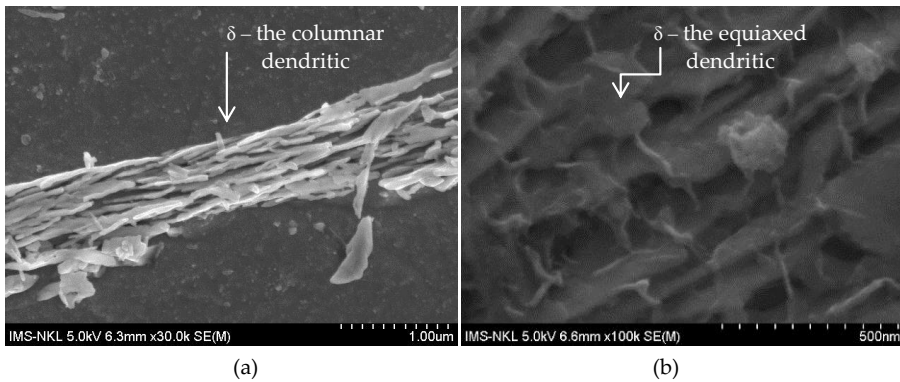


Figure 6: Structure of δ – Ferrite: (a) The columnar dendritic and (b) The equiaxed dendritic

The microstructure of the multi-pass weld was divided into individual beads (Figure 7a). A small zone along the fusion line showed the cellular morphologies of δ -Ferrite (Figure 7b); meanwhile, the columnar dendritic shape was considered as features extended from the fusion line of a weld pass toward the subsequent passes (Figure 7c). This can be explained due to the heat flow direction toward the surface of each bead.

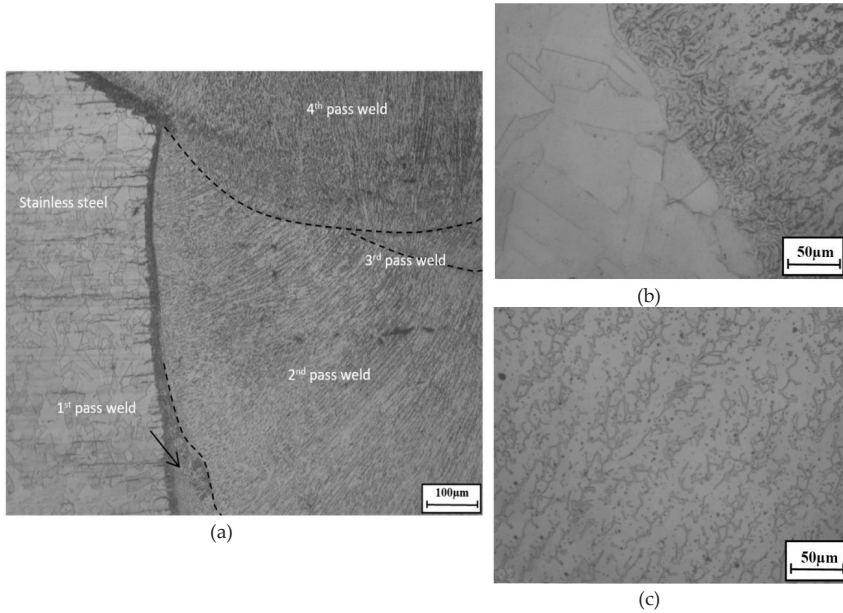


Figure 7: Microstructure in the fusion line of multi-pass welding: (a) Division the bead weld in the multi-pass welding, (b) Fine cellular δ -Ferrite along the fusion line and (c) Columnar dendritic δ -Ferrite in each bead weld

The scanning electron microscope showed clearly the shape of the columnar dendritic (Figure 8a) and the fine cellular with fine particles (Figure 8b). In fact, the formation of columnar dendritic and the fine cellular may be explained that the 1st pass weld is directly contacted with the base metal, thus, the grain has a small size with the very high cool rate. For the 2nd pass weld, the heat transfer rate decreases, leading to an increase in the grain size.

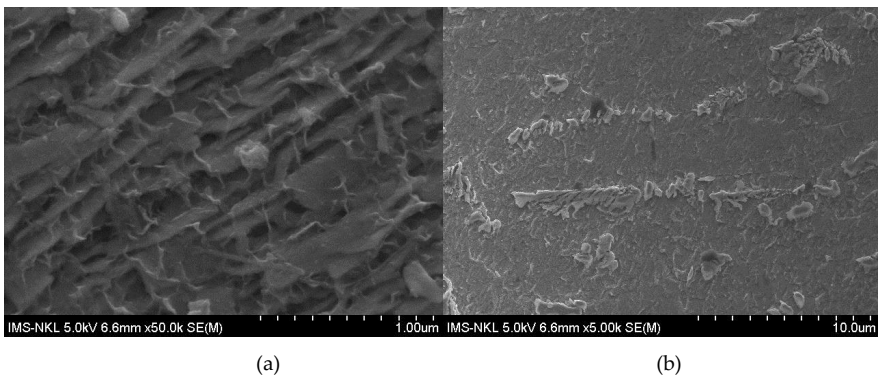
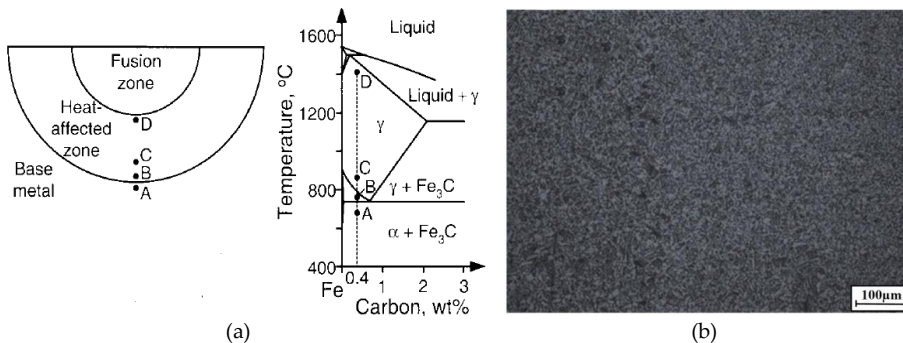


Figure 8: Structure of δ – Ferrite: (a) The columnar dendritic and (b) The equiaxed dendritic

3.3 The Recrystallization of the HAZ of Low-Carbon Steel Side

In terms of the single-pass welding, the HAZ in the low-carbon steel might correspond to the Fe-C phase diagram which is shown in Figure 9a. From Figure 9a, it can be seen that the gradual change in the grain size occurred from the fusion line to the base metal. Next fusion line, the average grain size was the largest (position D), and this grain size decreased at the base metal zone (position A). Widmanstatten Ferrite phases were thought to be formed along grain boundaries. Moreover, due to the variations of peak temperature, as well as the cooling rate, the Austenite phases were transformed to Martensite phases or Bainite phases. The differences in the HAZ of low-carbon steel zones are presented in Figure 9b, Figure 9c, and Figure 9d.

Based on the results of the microstructure analysis, Figure 9d (position D) shows that a direct contact with the fusion zone was very large. According to Figure 9a, at position D, the temperature was quite high (near the melting point). The optical microscope showed that the microstructure was the Ferrite and Martensite form with large size. This state affected the mechanical properties of the weld strongly. However, with position B (Figure 9b) and position C (Figure 9c), the particle sizes decreased. This is explained that position C and position B are far from the fusion zone, thus, the temperatures decrease, resulting in the small fine particle size due to recrystallization.



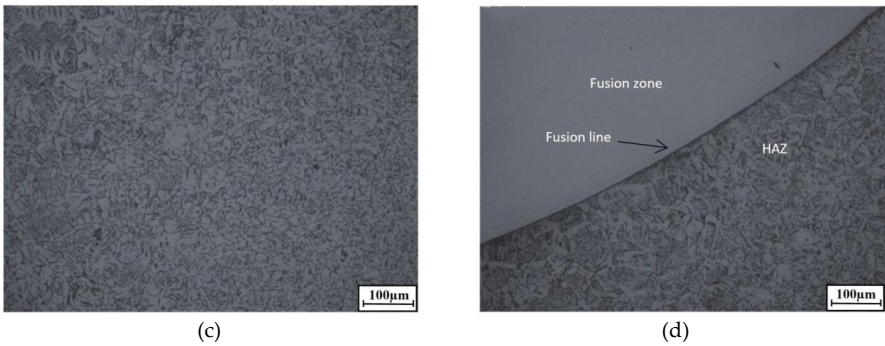


Figure 9: Carbon steel weld HAZ and the change in microstructure in the HAZ of single-pass welding: (a) Phase diagram [6], (b) Position B, (c) Position C and (d) Position D

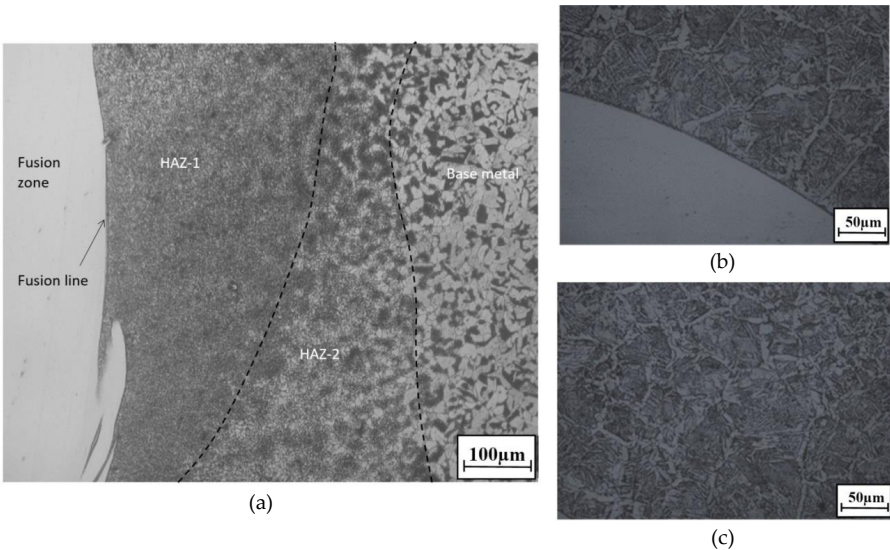


Figure 10: Microstructure in the HAZ: (a) The multi-pass welding; (b) HAZ-1 (x200) and (c) HAZ-2 (x200)

In addition, it can be seen from Figure 10a that there was a recrystallization in HAZ after conducting the second pass welding. For this reason, the multi-pass welding-based recrystallization was divided into two zones, including HAZ-1 and HAZ-2 (Figure 10b and Figure 10c). From Figure 10b, the formed grain-refining sizes, which were much finer than those of single-pass welding, could be clearly seen. This region is found to be a well-heated one with a high effectiveness because the heat treatment is conducted at the temperature over the critical temperature of ending-transformation of Austenite. This temperature allows the Austenite phase to be fully formed. Therefore, the decomposition and conversion of Austenite phase into the Martensite phase, Bainite

phase, or Pearlite phase, or Ferrite phase under the suitable cooling process can be indicated. Nonetheless, the peak temperature of this region is still higher than that of the critical temperature, and the gradual reduction of the temperature for the following pass results in the formation of Austenite grains with finer and finer nucleate. As a result, the above-mentioned Austenite grains decompose into smaller Pearlite phase and Ferrite phase without the Martensite phase and Bainite phase. Furthermore, from Figure 10c, the partial grain-refining zone subjected to a peak temperature was just higher than the effective critical temperature of beginning-transformation for Austenite, Pearlite and Ferrite grains with the extremely fine could be observed in HAZ-2. The occurrence of crystalline regions is due to the influence of temperature on different welding times. In the second welding layer, the HAZ region temperature of the first welding layer is again heated and then cooled. In the second heating times, the temperature decreases in comparison to the first one, the Austenite particles formed during the heating process are fine grains combined with the decrease of the cooling rate (due to the preheated welding plate), thus, the grain has a small size.

3.4 The Mechanical Properties of the HAZ of Low-Carbon Steel Side

In this part, mechanical properties of the HAZ of low-carbon steel including hardness, tensile strength, elastic strength, and elongation were tested. The hardness values of multi-pass welding in the various zones are shown in Figure 11 where the distribution of hardness profile for the single-pass welding was lower than that of multi-pass welding.

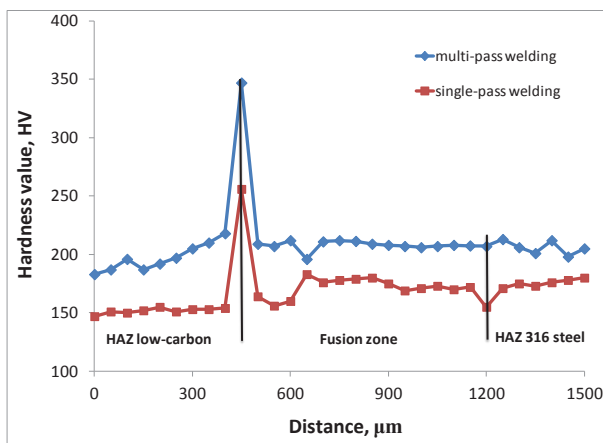


Figure 11: Hardness distribution profiles

From Figure 11, it can be seen in the HAZ that the Vickers hardness (HV) values of low-carbon steel, fusion zone, and 316 stainless steel were insignificantly changed, these hardness values fluctuated from 196HV to 212 HV for multi-pass welding, and from 155 HV to 183 HV for single-pass welding. However, for multi-pass welding, the hardness value for both cases in the fusion line of low-carbon steel side reached the highest value, corresponding to 350 HV. The hardness value of single-pass welding is lower than that of multi-pass welding because the released heat of the following pass in the multi-pass welding process is thought to provide more energy to the previous pass. Thus, the crystallization process takes place more slowly compared to the crystallization process of the single-pass welding where no heat is supplied subsequently. In addition, the formation of carbide phases contributes to the increase in the material hardness. Besides, the alloy element with high content, as well as the carbides which form more in the HAZ of low-carbon steel and fusion zone may be the main cause leading to the highest hardness. Nonetheless, more carbides in this region are also likely to damage the weld, and the heat treatment method may be used to overcome the above-mentioned damage and further investigation is needed.

After conducting the measurement of the tensile strength values, elastic strength, and elongation for single-pass welds and multi-pass welds, their values of mechanical properties are given in Table 3.

Table 3: The results of strength

Welding sample	Tensile strength (MPa)	Elastic Strength (MPa)	Elongation
Carbon steel	> 418	242	30
Single-pass welds	445	190	21
Multi-pass welds	529	221	15

The results of this study showed that the tensile strength of multi-pass welding was higher than that of single-pass welding and low-carbon steel. However, the elastic limit of the multi-pass welding was smaller than that of low-carbon steel. The elongation for multi-pass welding was also the lowest. This is perfectly consistent with above-studied results on microstructure. Moreover, with the single-pass welding, the recrystallization does not occur in the microstructure, thus, the mechanical properties decrease. In terms of elongation, for low-carbon steel, there is a maximum elongation because the microstructure is homogeneous, and it is not affected by the HAZ. Based on the test results of strength and the observed geometry of the test specimen, both samples were destroyed in the HAZ. This is due to the changes in microstructure in the HAZ, resulting in the accumulation of residual

stresses which cause the as-presented destruction. The analysis result for the microstructure in the destruction zone shows a break in the bonding between the metal particles which is considered the main cause of the material destruction in the HAZ.

4.0 CONCLUSION

In this study, the welds between 316 stainless steel and low-carbon steel were investigated on the basis of the microstructure and mechanical properties of the HAZ and fusion zone. Some findings are indicated as follows:

- i. There are differences in the microstructure between the multi-pass welding and the single-pass welding, where the bead welds with the columnar dendritic shape are extended from the fusion line of a weld pass toward the subsequent passes. Furthermore, the recrystallization occurring in the HAZ of low-carbon steel side is the main cause of the grain-refining/partial grain-refining zone formation.
- ii. The multi-pass welding shows the higher hardness value compared to the single-pass welding. The highest hardness value in the HAZ is 350 HV. However, the HAZ of carbon steel is found as the weakest zone, equal to 445 MPa of tensile strength for single-pass welding and 529 MPa of tensile strength for multi-pass welding. Meanwhile, the elastic strength and elongation of single-pass welding are 190 MPa and 21 MPa, the elastic strength and elongation of multi-pass welding are 221 MPa and 15 MPa, respectively.

REFERENCES

- [1] R. R. Mishra, V. K. Tiwari, and S. Rajesha, "A study of tensile strength of mig and tig welded dissimilar joints of mild steel and stainless steel," *International Journal of Advances in Materials Science and Engineering*, vol. 3, no. 2, pp. 23-32, 2014.
- [2] A. Aloraier, A. Al-Mazrouee, J. Price, and T. Shehata, "Weld repair practices without post weld heat treatment for ferritic alloys and their consequences on residual stresses: A review," *International Journal of Pressure Vessels and Piping*, vol. 87, no. 4, pp. 127-133, 2010.

- [3] M. Chiumenti, M. Cervera, A. Salmi, C. A. De Saracibar, N. Dialami, and K. Matsui, "Finite element modeling of multi-pass welding and shaped metal deposition processes," *Computer Methods in Applied Mechanics and Engineering*, vol. 199, no. 37-40, pp. 2343-2359, 2010.
- [4] A. T. Hoang, L. H. Nguyen, and D. N. Nguyen, "A Study of Mechanical Properties and Conductivity Capability of Cu-9Ni-3Sn alloy," *International Journal of Applied Engineering Research*, vol. 13, no. 7, pp. 5120-5126, 2018.
- [5] A. Elmesalamy, L. Li, J. Francis, and H. Sezer, "Understanding the process parameter interactions in multiple-pass ultra-narrow-gap laser welding of thick-section stainless steels," *The International Journal of Advanced Manufacturing Technology*, vol. 68, no. 1-4, pp. 1-17, 2013.
- [6] H. Fujii, Y. D. Chung, Y. F. Sun, and H. Tanigawa, "Interface shape and microstructure controlled dissimilar friction stir lap welded steels," *Science and Technology of Welding and Joining*, vol. 18, no. 4, pp. 279-286, 2013.
- [7] D. Kianersi, A. Mostafaei, and A. A. Amadeh, "Resistance spot welding joints of AISI 316L austenitic stainless steel sheets: Phase transformations, mechanical properties and microstructure characterizations," *Materials & Design*, vol. 61, pp. 251-263, 2014.
- [8] A. T. Hoang, D. N. Nguyen, V. V. Pham, "Heat treatment furnace for improving the weld mechanical properties: Design and fabrication," *International Journal of Mechanical Engineering & Technology*, vol. 9, no. 6, pp. 496-506, 2018.
- [9] G. Li, C. Zhang, M. Gao, and X. Zeng, "Role of arc mode in laser-metal active gas arc hybrid welding of mild steel," *Materials & Design*, vol. 61, pp. 239-250, 2014.
- [10] X. D. Pham, A. T. Hoang, and D. N. Nguyen, "A Study on the Effect of the Change of Tempering Temperature on the Microstructure Transformation of Cu-Ni-Sn Alloy," *International Journal of Mechanical & Mechatronics Engineering*, vol. 18, no. 4, pp. 27-34, 2018.
- [11] X. D. Pham, A. T. Hoang, D. N. Nguyen, and V. V. Le, "Effect of Factors on the Hydrogen Composition in the Carburizing Process," *International Journal of Applied Engineering Research*, vol. 12, no. 19, pp. 8238-8244, 2017.
- [12] J. Frostevarg, "Factors affecting weld root morphology in laser keyhole welding," *Optics and Lasers in Engineering*, vol. 101, no. 2, pp. 89-98, 2018.
- [13] A. Świerczyńska, J. Łabanowski, and D. Fydrych, "The effect of welding conditions on mechanical properties of superduplex stainless steel welded joints," *Advances in Materials Science*, vol. 14, no. 1, pp. 14-23, 2014.
- [14] A. S. Tremsin, S. Ganguly, S. M. Meco, G. R. Pardal, T. Shinohara, and W. B. Feller, "Investigation of dissimilar metal welds by energy-resolved neutron imaging," *Journal of Applied Crystallography*, vol. 49, no. 4, pp. 1130-1140, 2016.

- [15] C. Zhang, M. Gao, D. Wang, J. Yin, and X. Zeng, "Relationship between pool characteristic and weld porosity in laser arc hybrid welding of AA6082 aluminum alloy," *Journal of Materials Processing Technology*, vol. 240, no. 2 pp. 217-222, 2017.
- [16] F. Koch, M. Enderlein, and M. Pietrzyk, "Simulation of the temperature field and the microstructure evolution during multi-pass welding of L485MB pipeline steel," *Computer Methods in Materials Science*, vol. 13, no. 1-3, pp. 173-180, 2013.
- [17] N. Awang, M. H. F. Md Fauadi, A. Z. M. Noor, S. A. Idris, and N. S. Rosli, "An Improved Image Filtering Method for Weld Bead Inspection using Unsharp Masking Technique," *Journal of Advanced Manufacturing Technology*, vol. 12, no. 1(2), pp. 341-354, 2018.